DR PING CHENG (Orcid ID : 0000-0002-4232-9643)

Article type : Article

Enhanced thermal stability by introducing TiN diffusion barrier layer between W and SiC

Ping Cheng[1,2‡], Steven DelaCruz[2‡], Dung-Sheng Tsai[2], Zhongtao Wang[2], Carlo Carraro[2], Roya Maboudian[2,*]

[1]*National Key Laboratory of Science and Technology on Micro/Nano Fabrication, Department of Micro-Nano Electronics, Shanghai Jiao Tong University, Shanghai, 200240, People's Republic of China*

[2]*Department of Chemical and Biomolecular Engineering, University of California, Berkeley, California, 94720, United States*

* Corresponding author. maboudia@berkeley.edu

‡ Contributed equally to this work.

Abstract

The combination of W and SiC has many applications such as a hot cell of a thermionic energy converter, nuclear material and high temperature microelectronics. In this study, a 2μm thick TiN film is introduced as a diffusion barrier between SiC and W to avoid the inter-diffusion reaction at high temperature. The effect of annealing temperature on the surface morphology and microstructure of the TiN film is studied to explore its high temperature stability. Then 500nm W film is sputtered on the TiN film to characterize the inter-diffusion and stability of the W/TiN/SiC multilayer at 1100°C by XRD, Raman spectroscopy and cross-sectional EDS mapping techniques. The results indicate that the W/TiN/SiC multilayer is very stable even when heated at 1100°C for 25 hours.

Keywords: TiN film; diffusion barrier layer; W film; SiC; interface stability

1. Introduction

Silicon carbide (SiC) is a refractory compound semiconductor material that has many unique and desirable electrical, mechanical, and chemical properties including high melting point, low density, good mechanical behavior, resistance to oxidation at high temperature and chemical inertness to corrosive media. In addition to its application in high power electronic devices with the ability to operate at temperatures as high as 600ºC [1-3], SiC has several other high temperature applications including nuclear materials [4-6], reinforced composites [7], and the hot cell of thermionic energy converters [8-9].

Tungsten (W) is one of the preferred ohmic contact metals on SiC for semiconductor device applications due to its high melting point (3400ºC), high temperature stability, inherent heat resistance, high thermal conductivity as well as excellent corrosion and abrasion resistance [10-11]. In the thermionic energy converter (TEC), W is a good candidate for an emitter material, with SiC as a passivation layer against the combustion environment [8-9]. In high temperature gas cooled reactors (HTGRs), W has been considered to play a protective role for SiC, which could be used as an outer layer on the tristructural-isotropic (TRISO) particles [12-13]. Coating SiC with the W outer layer can improve the shielding effect, which allows for high burn up and enrichment without degrading the TRISO particles [14]. Although the combination of W/SiC has many applications, the inter-diffusion in SiC/W layers has been reported at elevated temperatures [10,12]. A variety of brittle tungsten silicides and carbides, such as W_2C, WSi_2, W_5Si_3 can form, leading to cracks and delamination upon thermal cycling.

TiN with a low electrical resistivity (several 10μΩ.cm), good hardness and chemical stability as well as a high melting point (≥3000°C), is used successfully as a super-hard coating for drilling or cutting tools, diffusion barrier and an adhesion-promoting layer between SiO_2 dielectric and Cu metallization layers in the micro-electronic industry [15]. In this study, TiN has been introduced as an effective diffusion barrier between SiC and W to avoid the inter-diffusion reaction under high temperature. The effect of annealing on the microstructure of TiN film and stability of the stacked structure W/TiN/SiC was

investigated by scanning electron microscopy (SEM), Raman spectroscopy and X-ray diffraction (XRD) methods.

2. Experimental procedure

A 4H-SiC(0001) wafer (SiCrystal AG) with a thickness of 350μm was used as the substrate. Before use, the substrate was cleaned with acetone, isopropanol, UV/ozone cleaner, HF solution and deionized water, sequentially. Both the TiN and W films were deposited using a load-locked 5kHz pulsed-DC sputter system with a sputter-etch capability (MRC 944). Prior to deposition, a pre-sputter process was carried out for 2 minutes to clean the contaminated surface of the target. The power for the pre-sputter process was 2 kW and the Ar pressure was 8mTorr. A sputter-etch process was performed with a 200 W power and an Ar pressure of 12 mTorr for 2 minutes to clean the substrate and enhance the adhesion between the film and the substrate. For the film deposition, the base pressure was about 5×10^{-7} mTorr and the working pressure was 8 mTorr. For the TiN film deposition, a power of 2 kW was applied to the Ti target and the reactive sputtering was carried out in a mixture gas of 25%N_2/75%Ar. The substrate was moved back and forth with a scan speed of 50cm/min to enhance the uniformity of the film. The thickness of the TiN film was about 2 μm. The TiN films were then placed in a hot-wall tube furnace (Thermo Scientific Lindberg Blue M) that was evacuated to a base pressure of 30 mTorr. Annealing was done under a constant flow of Ar at 500, 800 and 1100°C for 2 hours. The W film was sputtered on the TiN film on 4H-SiC substrate. A

power of 1 kW was applied to the W target. The thickness of the W film was about 500 nm.

SEM images were acquired by a field-emission SEM (FEI Quanta 3D FEG), which combined a field-emission SEM column, a Ga^+ FIB column (liquid-metal ion source), and an X-ray energy-dispersive spectrometry (EDS) column in one tool. The cross section of the W/TiN/SiC multilayer was exposed by a FIB milling. Then the SEM image and EDS mapping were obtained in the same tool. The crystal structure of the film was identified using an advanced X-ray diffractometer (Bruker AXS D8 Discover GADDS), which was operated at 35kV/40mA with a CoKα wavelength of 1.79Å. Raman spectra of the samples were acquired using a JYHoriba LabRAM spectrometer in backscattering configuration (excitation line: 632.817 nm, laser power at the sample: ≤4 mW, beam spot: ~1 μm).

3. Results and Discussion

The effects of deposition process parameters and post annealing on the microstructures and properties of TiN films deposited on Si or SiO_2 substrates with a thickness in nanometer scale have been extensively investigated [15-17]. However, the highest working temperature for the multilayer W/TiN/SiC in this study is above 1000°C, which is much higher than that used in traditional applications of TiN films in microelectronics (normally below 700°C). Thus, a wide range of annealing temperature (500-1100°C) was used for TiN films deposited on SiC substrate in this study. The effect

of annealing temperature on the composition and microstructure of TiN film on the SiC substrate was studied firstly, which is particularly important for the high temperature stability of the TiN diffusion barrier layer. Then, the W film was sputtered on the TiN/SiC bilayer to explore the microstructure, diffusion and stability of the multilayer W/TiN/SiC annealed at 1100°C.

For a standard powder TiN sample, there are four peaks due to the (111), (200), (220) and (311) planes, respectively. Among them, the (200) plane has the highest intensity. The (220) intensity is 45% of the (111) intensity in a powder diffractogram. Fig. 1 shows the XRD patterns of the 2μm thick TiN films as deposited and annealed. The peaks at 2θ= 42.5°and 73.2° are attributed to (111) and (220) planes of face-centered cubic (fcc) TiN, respectively. The data show that there exists strong (111) preferred crystallographic orientation, which was commonly found for physical-vapor deposited TiN thin films [18]. The preferred orientation of TiN films is determined by the competition between the surface energy and the strain energy [19]. Different from monoatomic fcc crystals, the (111) plane in TiN crystal with NaCl-type fcc structure has the lowest strain energy, whereas the (200) plane has the lowest surface energy. The surface energy stays nearly constant while the strain energy varies with the sputtering process parameters and film thickness [20]. The increasing rate of the strain energy, which is dependent on the plane (hkl), is larger on the (200) plane than on the (111) plane. In this study, the strain energy became dominant due to the large film thickness and high bombardment energy (2 kW)

of the deposited particles, and the (111) preferred orientation was observed according to the energy minimization rule. For the annealed TiN film, the (111) diffraction peaks are shifted from 2θ=42.5° to 42.9°, which has the same variation trend as that reported by other 21]. This implies that the post annealing reduces the lattice parameter of the TiN film, which is probably attributed to out-diffusion of the implanted sputter gases and the decrease of residual strain and other defects. When the annealing temperature is increased from 500 to 1100 °C, the preferred orientation does not change but the intensity of the peak and the grain size increases. Both the grain size and lattice strain are estimated using Williamson-Hall method. For the as-deposited and annealed TiN films at 500, 800 and 1100°C, the grain size is about 17, 27, 30 and 53nm, while the strain was 0.397%, 0.228%, 0,148% and 0.096%, respectively.

Fig.2 (a) shows Raman spectra of the 2μm TiN films annealed at different temperatures. The scattering peaks in the acoustic range (~150–300 cm^{-1}, TA and LA) and the optical range (400–650 cm^{-1}, TO and LO) mainly resulted from Ti ion vibrations and N ion vibrations, respectively [22-23]. The scattering at around 410 cm^{-1} between the acoustic and optical modes is in a frequency range corresponding to 2TA modes（2x~205 cm^{-1}）related to the stoichiometric defects. To further analyze the Raman spectra of TiN/SiC films, they were fitted at about 205, 310, 410, 550 and 670 cm^{-1}, which are assigned to the TA mode, LA mode, 2TA mode, TO mode and LO mode of TiN, respectively [22, 24]. Fig. 2 (b) shows the deconvolution results of the TiN/SiC film

annealed at 1100 ℃. The Raman peak at 130cm $^{-1}$ is assigned to the E_g mode of TiO_2, which means that even in dry Ar environment the oxidation of TiN films could occur at 1100 ℃ in our vacuum system. The peak area ratios of LO and 2TA to LA at different annealing temperatures were further estimated, as shown in Fig.2 (c). As the annealing temperature increased from 800 to 1100 ℃, the peak area ratio of LO to LA decreased rapidly, indicating replacement of nitrogen atoms in the TiN matrix by oxygen atoms [25]. The peak area ratio 2TA/LA of the TiN/SiC film annealed at 1100℃ was much greater than that of the other samples, indicating that stoichiometric defects increased after high temperature annealing [24].

Fig. 3 shows the surface micrographs of the TiN films deposited on the 4H-SiC substrate after annealing at temperatures between 500 and 1100 °C for 1 h. It was found that both the as-deposited TiN film and the film annealed at 500 °C display a homogenous crack-free surface consisting of a large number of microparticles. However, micro-cracks appear on the TiN films annealed at 800 and 1100 °C, which result from the thermal mismatch, the sputtering residual stresses and shrinkage produced during sintering. When the annealing temperature increased from 800 to 1100°C, the width of some cracks increased, and the microparticles agglomerated and were sintered into smooth blocks. The EDS analysis was carried out to determine the elemental composition of the TiN films. The molar ratio of Ti/N from EDS results for the as-deposited TiN film and the ones annealed at 500, 800 and 1100°C was 1, 1.02, 1.05 and 1.07, respectively.

In order to explore the stability of W/TiN/SiC multilayers under high temperature, a 500nm thick W film was sputtered on the as-deposited or annealed TiN films. Then all the samples were annealed at 1100°C for 1h in a flow of Ar gas. The SEM images of the 500nm W samples are shown in Fig.4. There are no cracks on the surfaces of W films whether or not the TiN film was annealed at 500°C. When the TiN films were annealed at 800 and 1100°C, the cracks on the surface of the W film are much smaller than those in the TiN film. This is probably attributed to the W layer developing high compressive stresses on cooling from the deposition temperature since the thermal expansion coefficient of W (4-6 ppm $°C^{-1}$) is smaller than that of TiN (9.4 ppm $°C^{-1}$).

Fig.5 shows XRD patterns of 500nm thick W films deposited on TiN/SiC annealed at 1100°C for different hours. The peak at $2\theta=47.1°$ is attributed to the (110) plane of $\alpha-W$ crystal representing a thermodynamically stable phase with bcc configuration. The W films have a strong (110) preferred orientation, which is in agreement with the results of W film deposited on (100) and (111) Si substrates [26]. It was reported that the (110) planes had the smallest surface energy than other grain planes for monoatomic bcc crystals [27]. Therefore grains will preferentially grow up in the <110> direction. No other peaks are detected even when the W/TiN/SiC multilayer is annealed at 1100°C for 25 hours, which indicats that the multilayer shows high stability even at 1100°C.

In order to observe the effect of the TiN layer on the diffusion between W and SiC at high temperature, the cross sections of the W/TiN/SiC multilayers annealed at 1100°C for

25 hours were exposed using FIB milling. Fig.6 shows the cross-sectional image and EDS mapping of the W/TiN/SiC sample annealed at 1100°C for 25 hours, for which the TiN film on SiC substrate was annealed at 500°C for 1h in a flow of argon before the W film was sputtered. There are no cracks for the W/TiN/SiC multilayer annealed at 1100°C for 25 hours. Additionally, there is no elemental inter-diffusion between the interface of W/TiN and TiN/SiC, which verifies that the TiN layer effectively prevented the formation of the silicides or carbides.

Fig.7 shows the cross-sectional image and EDS mapping of the W/TiN/SiC sample annealed at 1100°C for 25 hours, for which the TiN film on SiC substrate was annealed at 1100°C for 1h before the W film was sputtered. The longitudinal cracks occurred on the cross section of 2 μm thick TiN film, which is in agreement with the result in Fig.4 (d). However, neither the W diffusion into the TiN cracks nor the inter-diffusion between the W/TiN and TiN/SiC occurred for the W/TiN /SiC multilayer annealed at 1100°C for 25 hours. This also confirms the barrier effect of the TiN layer on the inter-diffusion between W and SiC.

4. Conclusion

In this study, a 2 μm thick TiN film is introduced as the diffusion barrier layer between SiC and W under high temperatures. The surface morphology and crystal structure of the TiN film annealed at different temperatures in a flow of Ar was characterized by XRD, Raman spectroscopy and SEM methods to explore its high

temperature stability. The results indicate that the TiN film shows (111) preferred orientation, which becomes stronger with increasing the annealing temperature. The cracks appeared on the surface of the TiN film due to thermal mismatch between the TiN film and SiC substrate when the annealing temperature was above 800°C. However, the cracks occurred on the surface of the W/TiN/SiC multilayer only when the annealing temperature was 1100°C. The stability of the W/TiN/SiC multilayer at 1100°C was investigated by XRD, Raman spectroscopy and cross-sectional EDS mapping techniques. The results indicated that the introduction of TiN film between W and SiC effectively prevents the inter-diffusion and improves the high temperature stability of the W/SiC, providing more opportunities for its use in high temperature applications.

Acknowledgements

This work was supported by the Advanced Research Projects Agency-Energy (ARPA-E), U.S. Department of Energy, under Award No. DE-AR0000664. Sputtering was performed in the UC Berkeley Marvell Nanofabrication laboratory. Work at the Molecular Foundry was supported by the Office Science, office of Basic Energy Sciences, of the U.S. Department of Energy under Contract No. DE-AC02-05CH11231.

References

[1] Tolbert LM, Zhang H, Chinthavali MS, Ozpineci B. SiC-based power converters. Mater Sci Forum 2007; 556-557: 965-970

[2] Kumar A, Aspalli MS. SiC: An advanced semiconductor material for power devices.

Intl J Res Eng Tech. 2014; 3: 248-252

[3] Seal S, Mantooth HA. High Performance Silicon Carbide Power Packaging-Past Trends, Present Practices, and Future Directions. Energies. 2017; 10:341

[4] Kishimoto H, Shibayama T, Abe T, Shimoda K, Kawamura S, Kohyama A. Diffusion Bonding Technology of Tungsten and SiC/SiC Composites for Nuclear Applications. IOP Conf Ser: Mater Sci Eng. 2011; 18: 162015.

[5] Malherbe JB, Berg NG, Kuhudzai RJ, Hlatshwayo TT, Thabethe TT, Odutemowo OS. Scanning electron microscopy of the surfaces of ion implanted SiC Nucl Instrum Methods Phys Res, Sect B, 2016; 354: 23–27.

[6] Friedland E, G¨artner K, Hlatshwayo TT, Berg NG, Thabethe TT. Influence of radiation damage on xenon diffusion in silicon carbide. Nucl Instrum Methods Phys Res, Sect B, 2014; 332: 415–420.

[7] Guo C, Zhang C, He L, Jin B, Shi N. Microstructure Characterization of Long W Core SiC Fiber. J Mater Sci Technol, 2007; 23: 677–684.

[8] Khalid KAA., Leong TJ, Mohamed K. Review on Thermionic Energy Converters. IEEE Trans Electron Dev. 2016; 63(6): 2231-2241.

[9] DelaCruz S, Wang ZT, Cheng P, Carraro C, Maboudian R. TiN diffusion barrier for stable W/SiC(0001) interfaces in inert ambient at high temperature. Thin Solid Films. 2019;670 (31):54-59.

[10] Rogowskia J, Kubia A. Effects of annealing temperature on the structure and

electrical properties of tungsten contacts to n-type silicon carbide. Mater Sci Eng B 2015; 191: 57–65

[11] Geib KM, Mahan JE, Wilmsen CW. W/SiC Contact Resistance at Elevated Temperatures. Springer, Berlin, Heidelberg, 1989;43:224-228

[12] Thabethe TT, Hlatshwayo TT, Njoroge EG, Nyawo TG, Ntsoane TP, Malherbe JB. Interfacial reactions and surface analysis of W thin film on 6H-SiC. Nucl. Instrum. Methods Phys Res, Sect B 2016; 371: 235–239

[13] Thabethe TT, Njoroge EG, Hlatshwayo TT, Ntsoane TP, Malherbe JB. Surface and interface structural analysis of W deposited on 6H–SiC substrates annealed in argon. RSC Adv, 2017; 7: 2 -7

[14] Kishimoto H, Shibayama T, Shimoda K, Kobayashi T, Kohyama A. Microstructural and mechanical characterization of W/SiC bonding for structural material in fusion. J Nucl Mater 2011; 417: 387–390

[15] Ponon NK, Appleby DJR, Arac E, King PJ, Ganti S, Kwa KSK, et al. Effect of deposition conditions and post deposition anneal on reactively sputtered titanium nitride thin films. Thin Solid Films 2015; 578: 31–37

[16] Popović M，Novaković M , Bibić N. Annealing effects on the properties of TiN thin films. Process Appl Ceram 2015; 9 (2): 67–71

[17] Bavadi R, Valedbagi S. Physical properties of titanium nitride thin film prepared by DC magnetron sputtering. Mater Phys Mech 2012; 15: 167-172

[18] Machunze R., Janssen GCAM. Stress and strain in titanium nitride thin films. Thin Solid Films 2009; 517: 5888–5893

[19] Oh UC., Je JH. Effects of strain energy on the preferred orientation of TiN thin films. J Appl Phys 1993; 74: 1692-1696

[20] Zhao JP, Wang X, Chen ZY, Yang SQ, Shi TS, Liu XH. Overall energy model for preferred growth of TiN films during filtered arc deposition. J Phys D: Appl Phys. 1997; 30: 5–12.

[21] Bunjongpru W, Sungthonge A, Porntheeraphat S, Rayanasukha Y, Pankiew A, Jeamsaksiri W, et al. Very low drift and high sensitivity of nanocrystal-TiO_2 sensing membrane on pH-ISFET fabricated by CMOS compatible process. Appl Surf Sci. 2013; 267: 206–211

[22] Chen CC., Liang XT, Tse WS, Chen IY, Duh. JG. Raman Spectra of Titanium Nitride Thin Films, Chin J Phys. 1994; 32: 205-210.

[23] Cheng YH, Tay BK, Lau SP, Shi X. Raman Spectroscopy and X-ray Diffraction Studies of (Ti, Al) N Films Deposited by Filtered Cathodic Vacuum Arc at Room Temperature, J Appl Phys. 2001; 89: 6192-6197.

[24] Constable CP, Yarwood J, Munz WD. Raman Microscopic Studies of PVD Hard Coatings, Surf Coat Technol. 1999;116–119:155-159.

[25] Barshilia HC, Rajam KS. Raman Spectroscopy Studies on the Thermal Stability of TiN, CrN, TiAlN Coatings and Nanolayered TiN/CrN, TiAlN/CrN Multilayer Coatings, J

Mater Res. 2004; 19: 3196-3205.

[26] Mamor M, Dufour-Gergam E, Finkman L, Tremblay G, Meyer F, Bouziane K. WSi Schottky diodes: effect of sputtering deposition conditions on the barrier height. Appl surf Sci. 1995; 91:342-346

[27] Wang SG, Tian EK., Lung CW. Surface energy of arbitrary crystal plane of bcc and fcc metals. J Phys Chem Solids 2000; 61: 1295–1300.

Figure and/or Table Caption List

Fig.1 XRD patterns of the 2um TiN films annealed at different temperature.

Fig.2 (a) Raman spectra of the 2um TiN films annealed at different temperature; (b) Typical deconvolution spectrum of the TiN film annealed at 1100°C; (c) Temperature-dependent peak area ratio of TiN/SiC Raman vibration mode (LO to LA and 2TA to LA).

Fig.3 SEM images of 2um TiN films annealed at different temperature. (a) As deposited; (b) 500°C; (c)800°C (d)1100°C.

Fig.4 SEM images of 500nm W films sputtered on the different TiN film when annealed at 1100°C for 1h in a flow of Ar.（a）As-deposited TiN film; (b) TiN film annealed at 500°C; (c) TiN film annealed at 800°C; (d) TiN film annealed at 1100°C

Fig. 5 XRD patterns of 500nm thick W film deposited on TiN/SiC. (a) As deposited; (b)Annealed at 1100°C for 1h; (c) Annealed at 1100°C for 25h.

Fig.6 Cross-sectional SEM image and EDS mapping of the sample (W/ annealed TiN film at 500°C/SiC) after annealed at 1100°C for 25h

Fig.7 Cross-sectional SEM image and EDS mapping of the sample (W/ annealed TiN film at 1100°C/SiC) after annealed at 1100°C for 25h

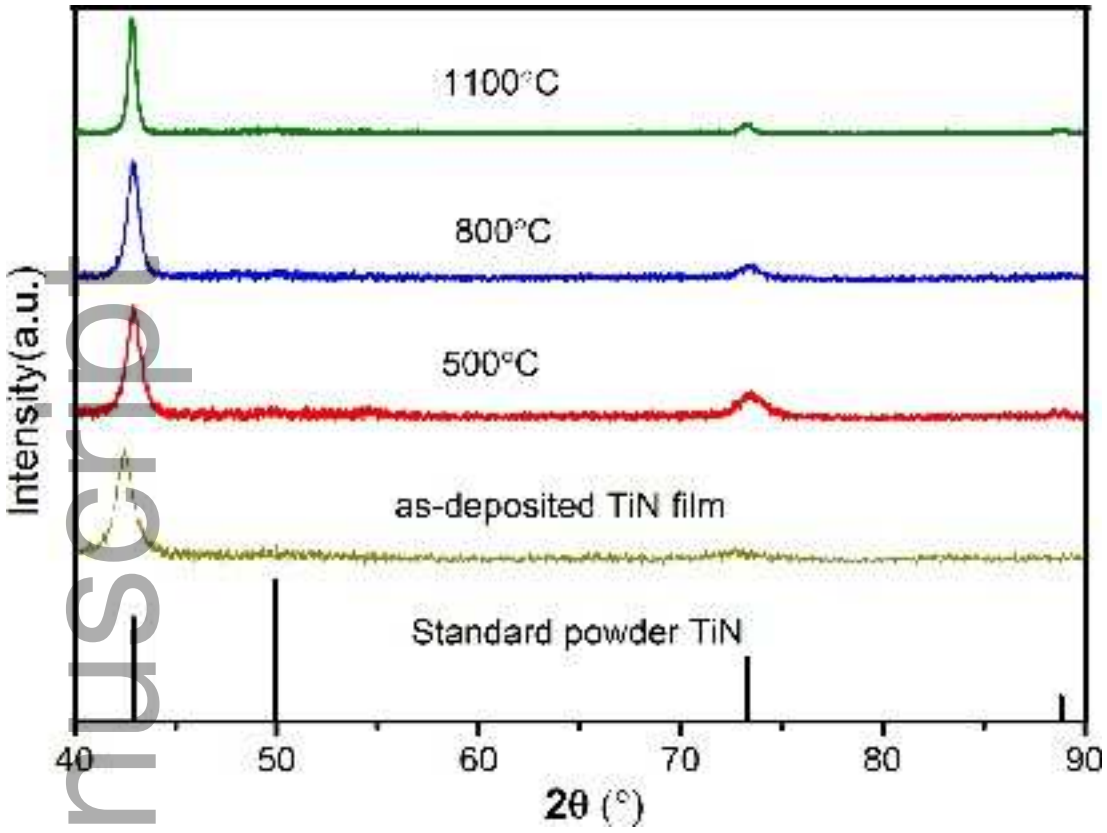

jace_16392_f1.tif

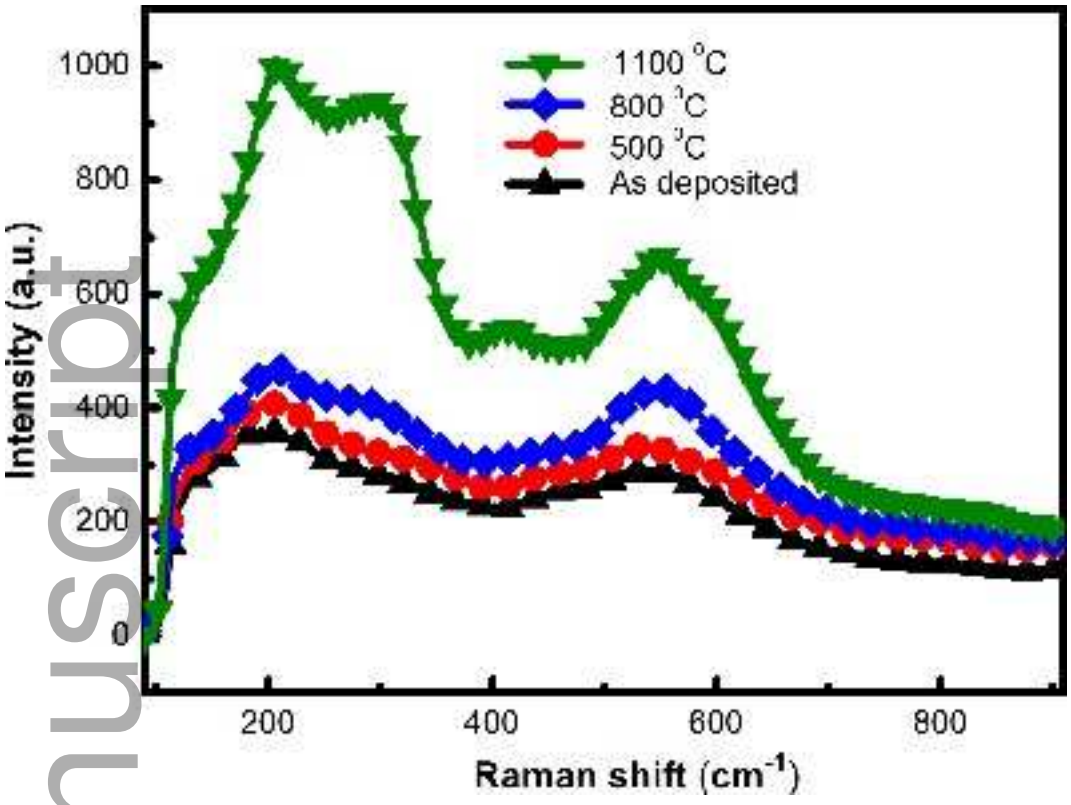

jace_16392_f2a.tif

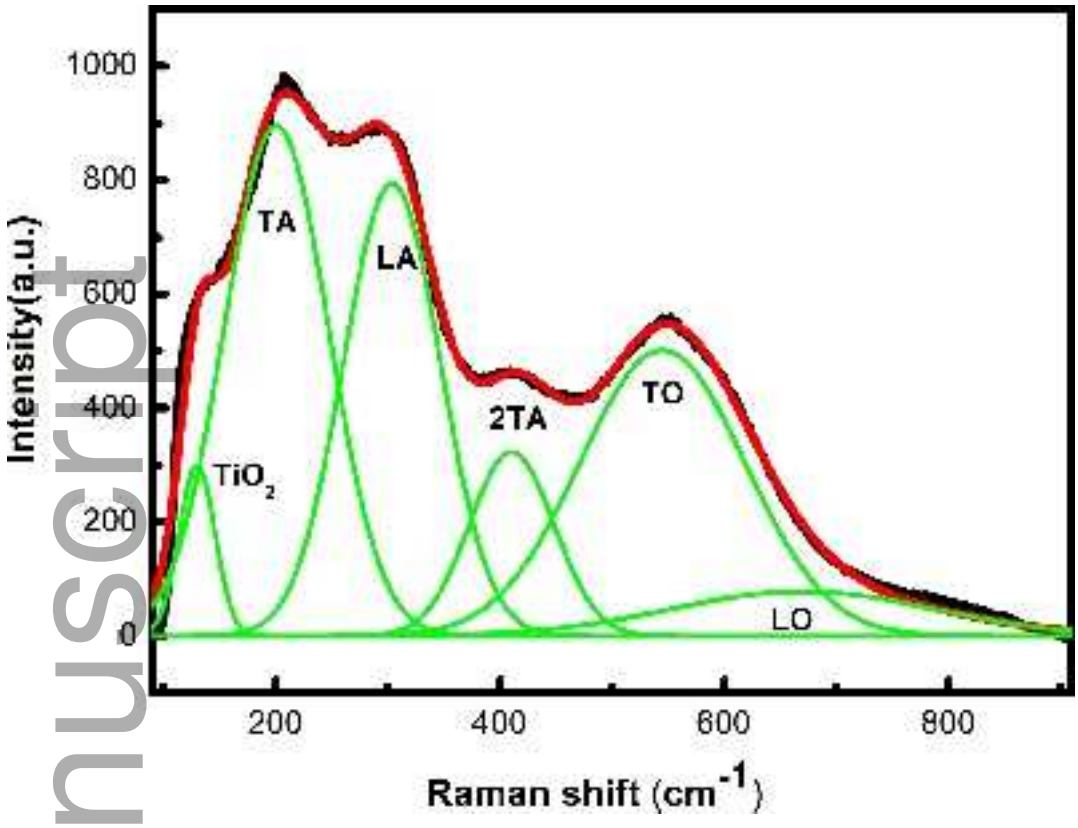

jace_16392_f2b.tif

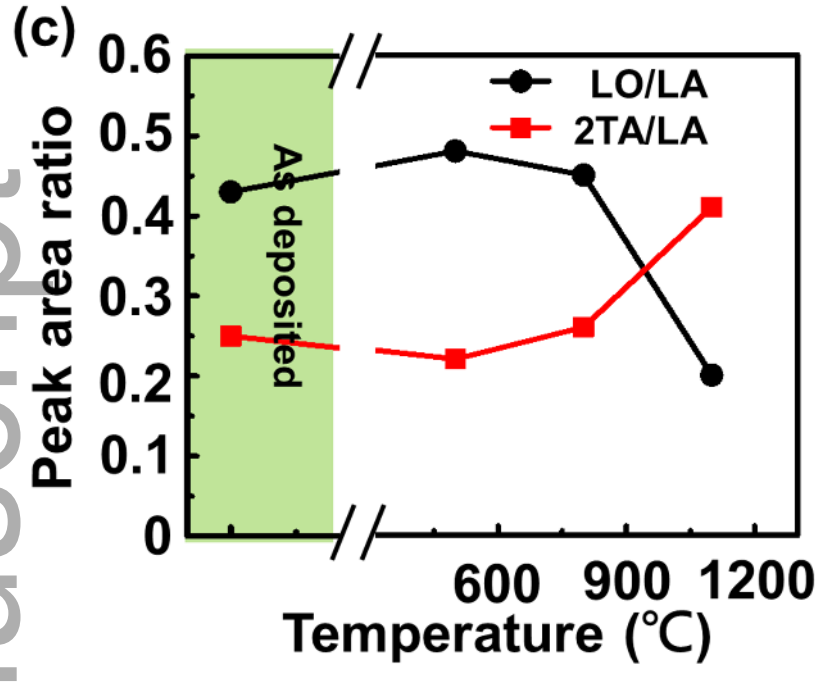

jace_16392_f2c.tif

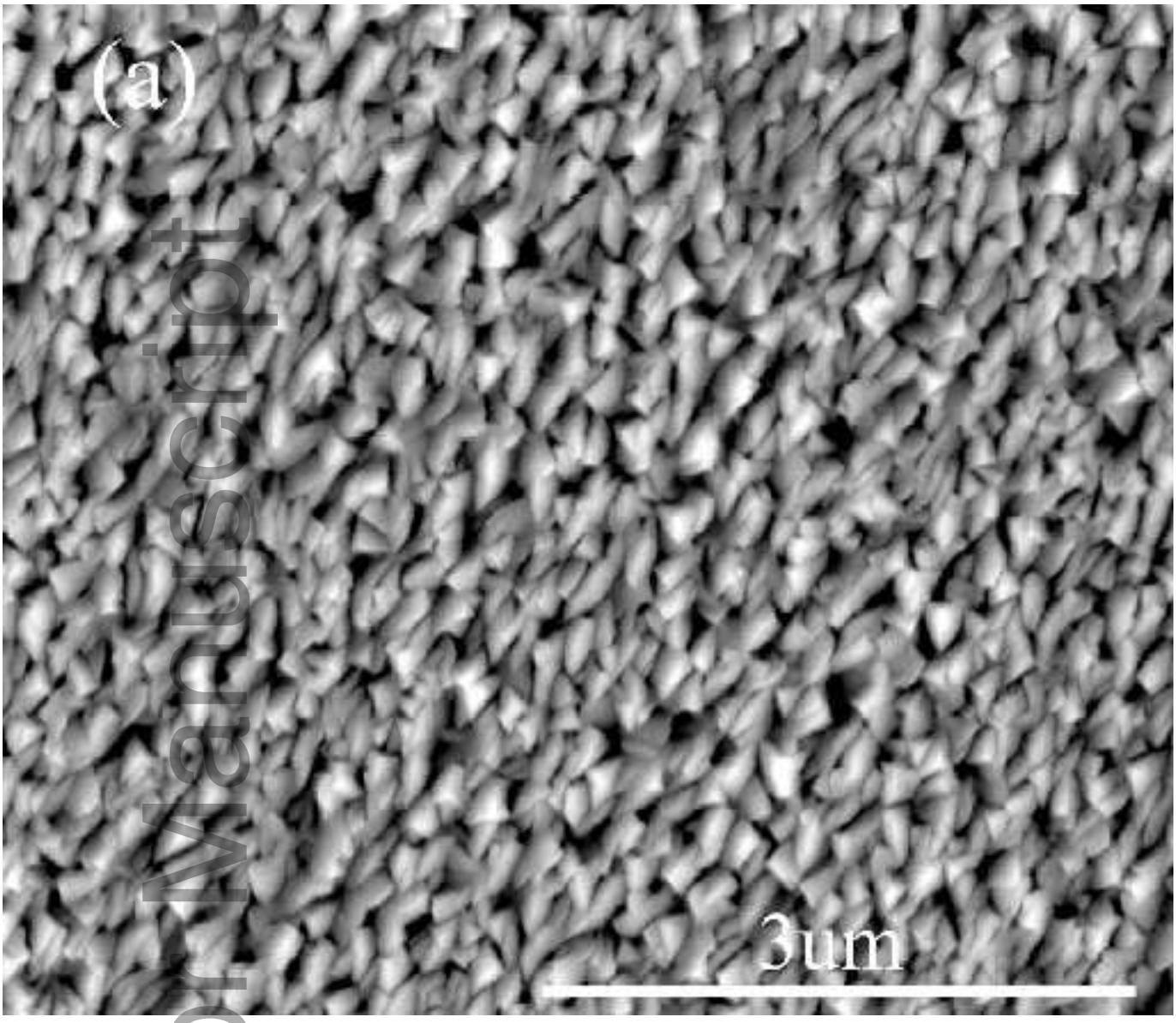

jace_16392_f3a.tif

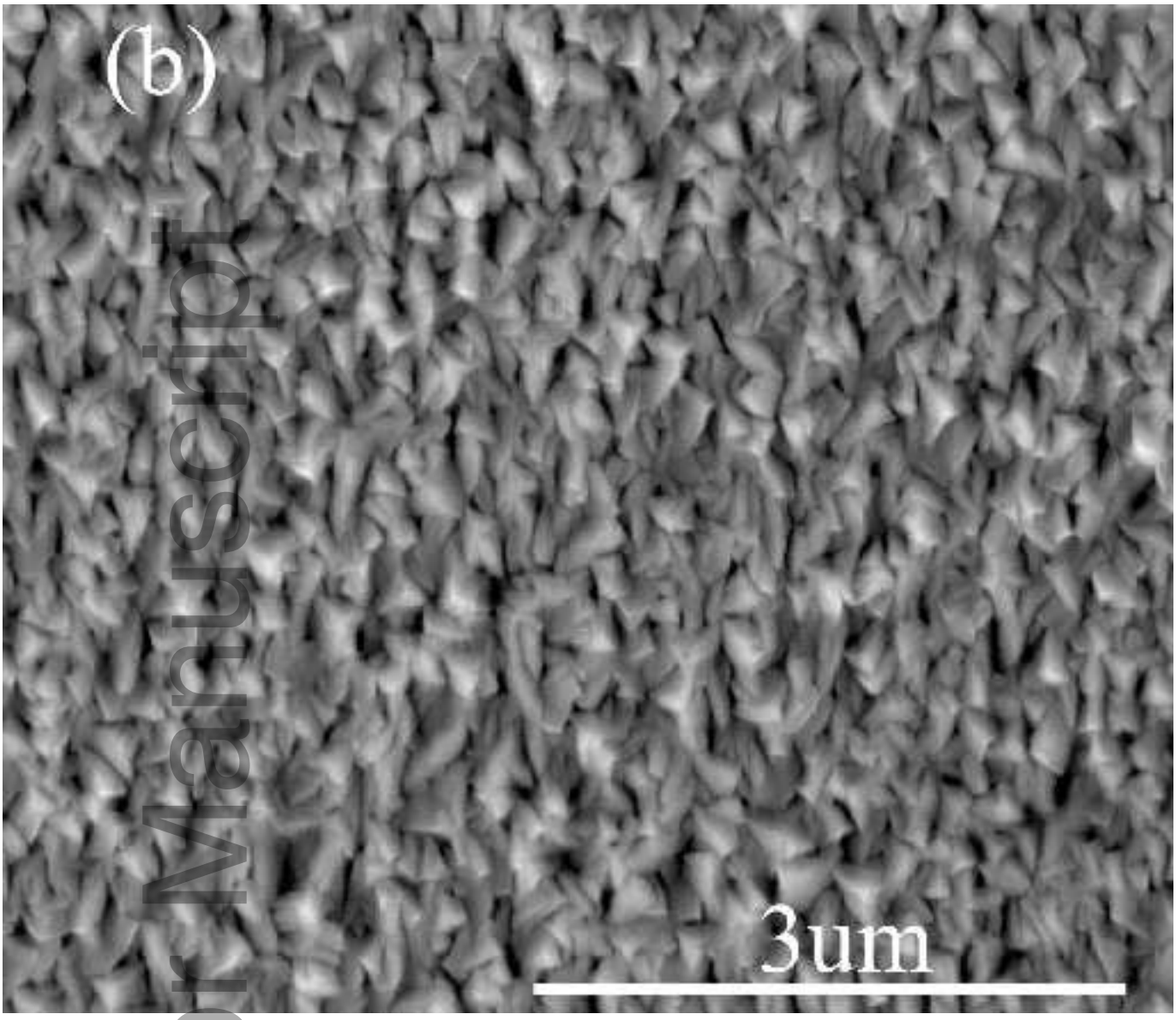

jace_16392_f3b.tif

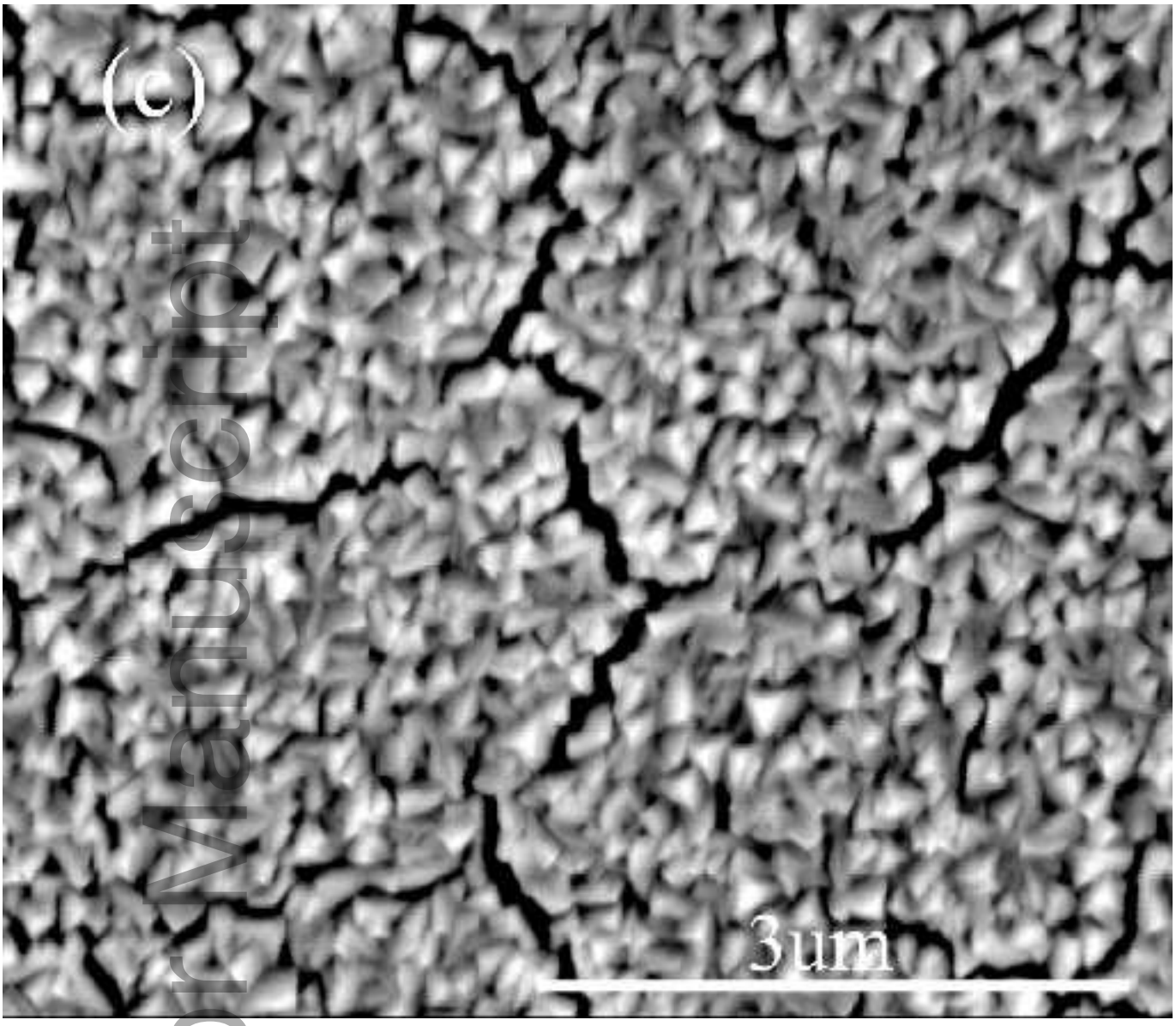

jace_16392_f3c.tif

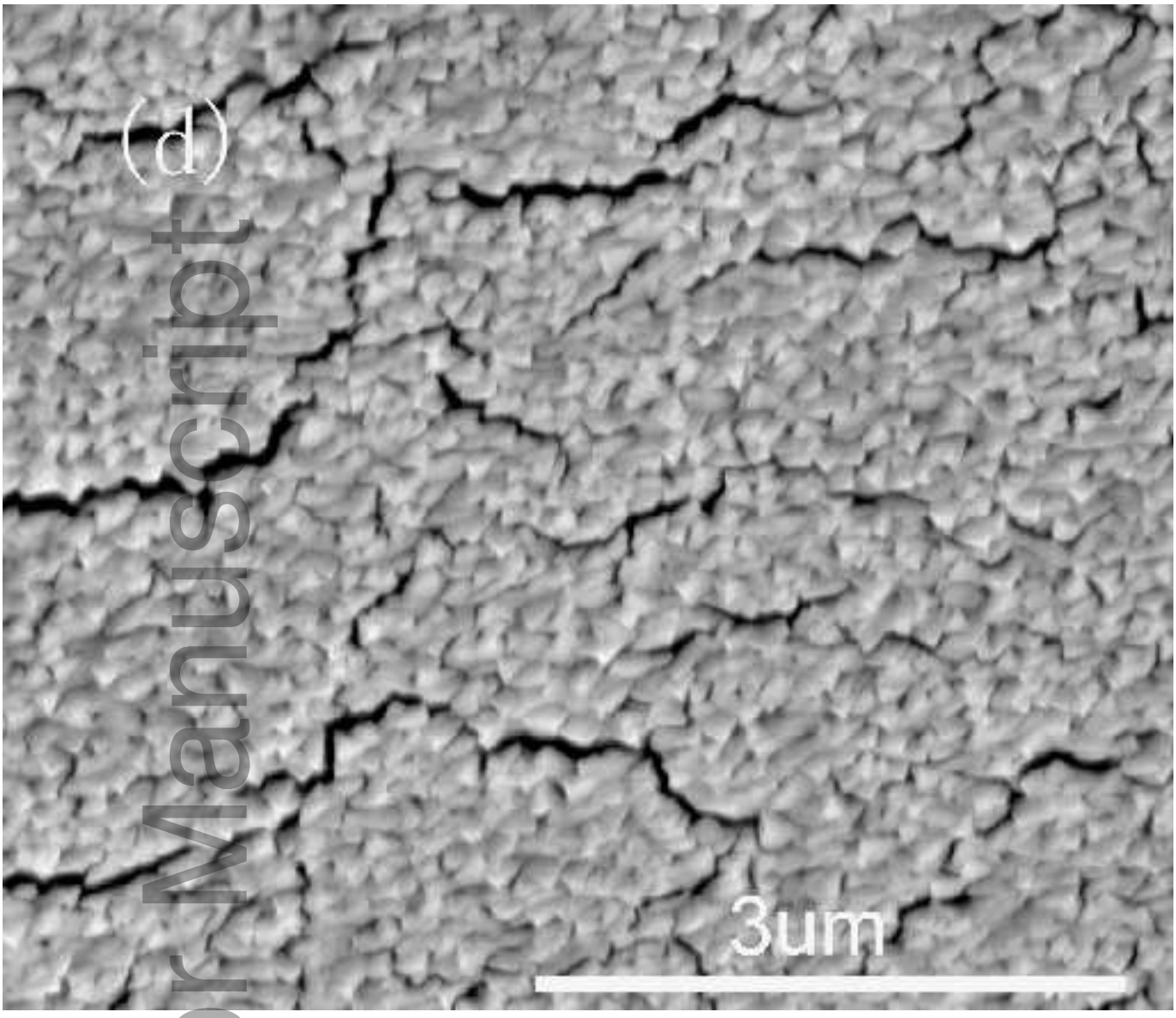

jace_16392_f3d.tif

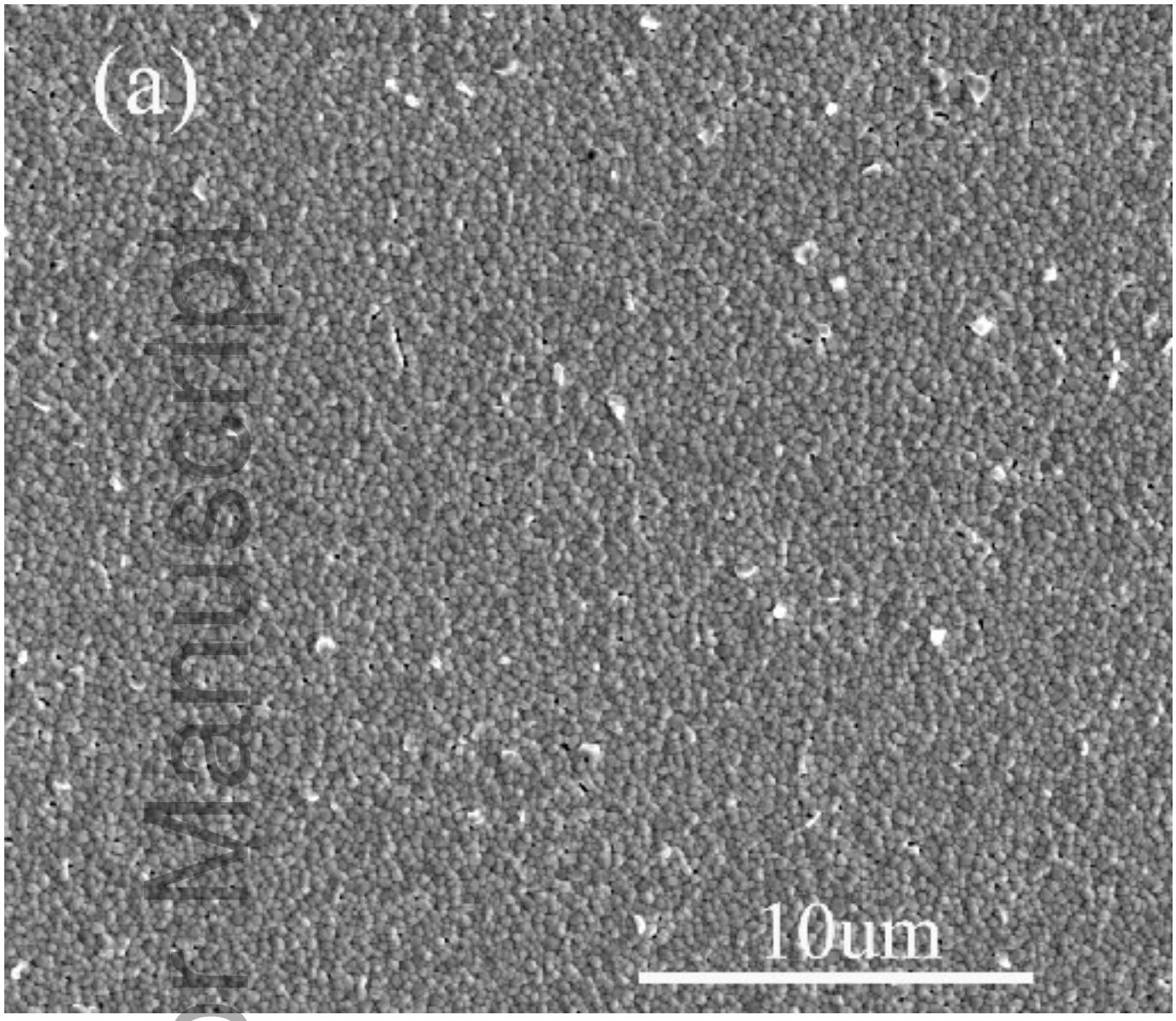

jace_16392_f4ï¼ˆaï¼‰-2.tif

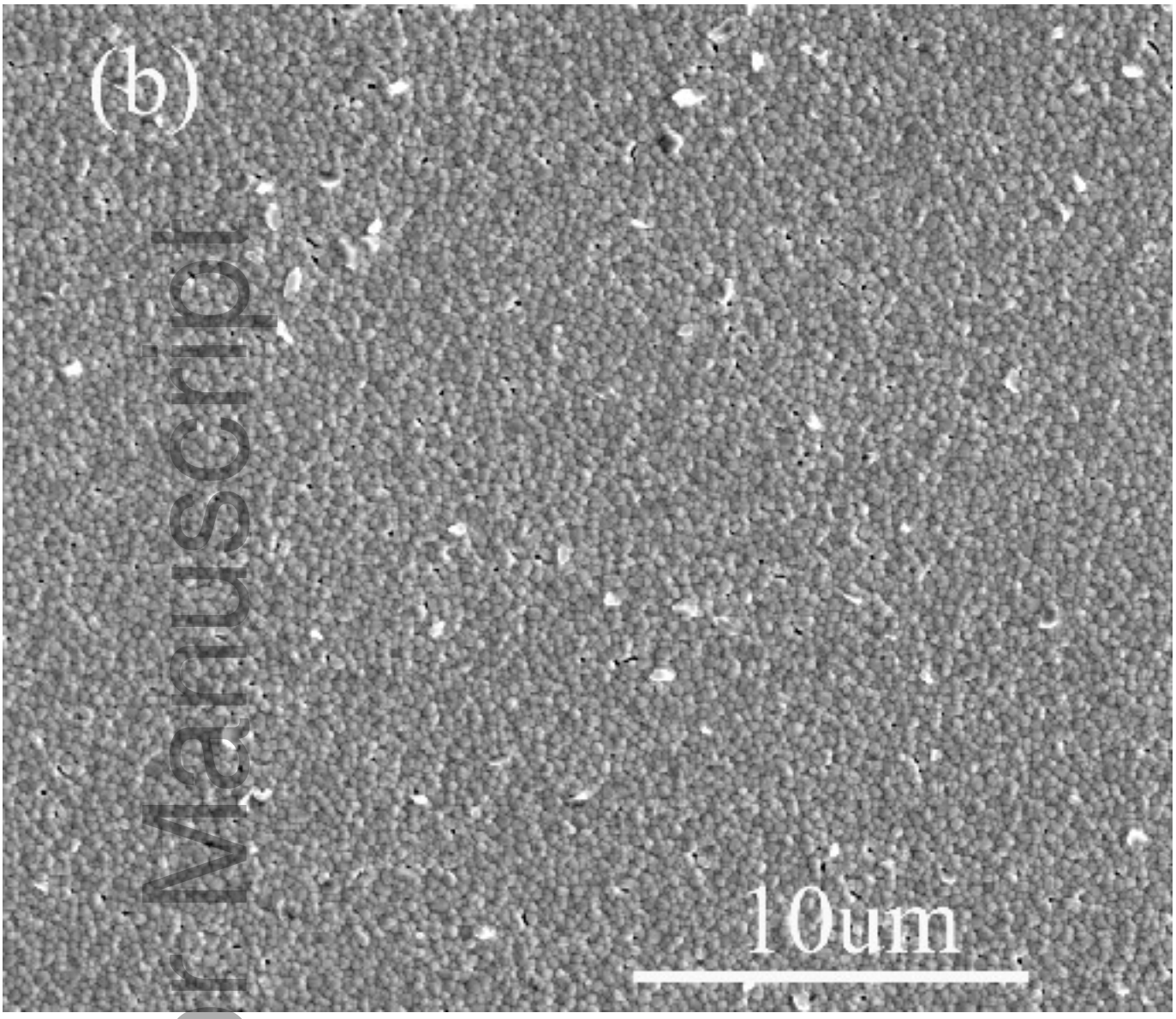

jace_16392_f4ï¼ˆbï¼‰.tif

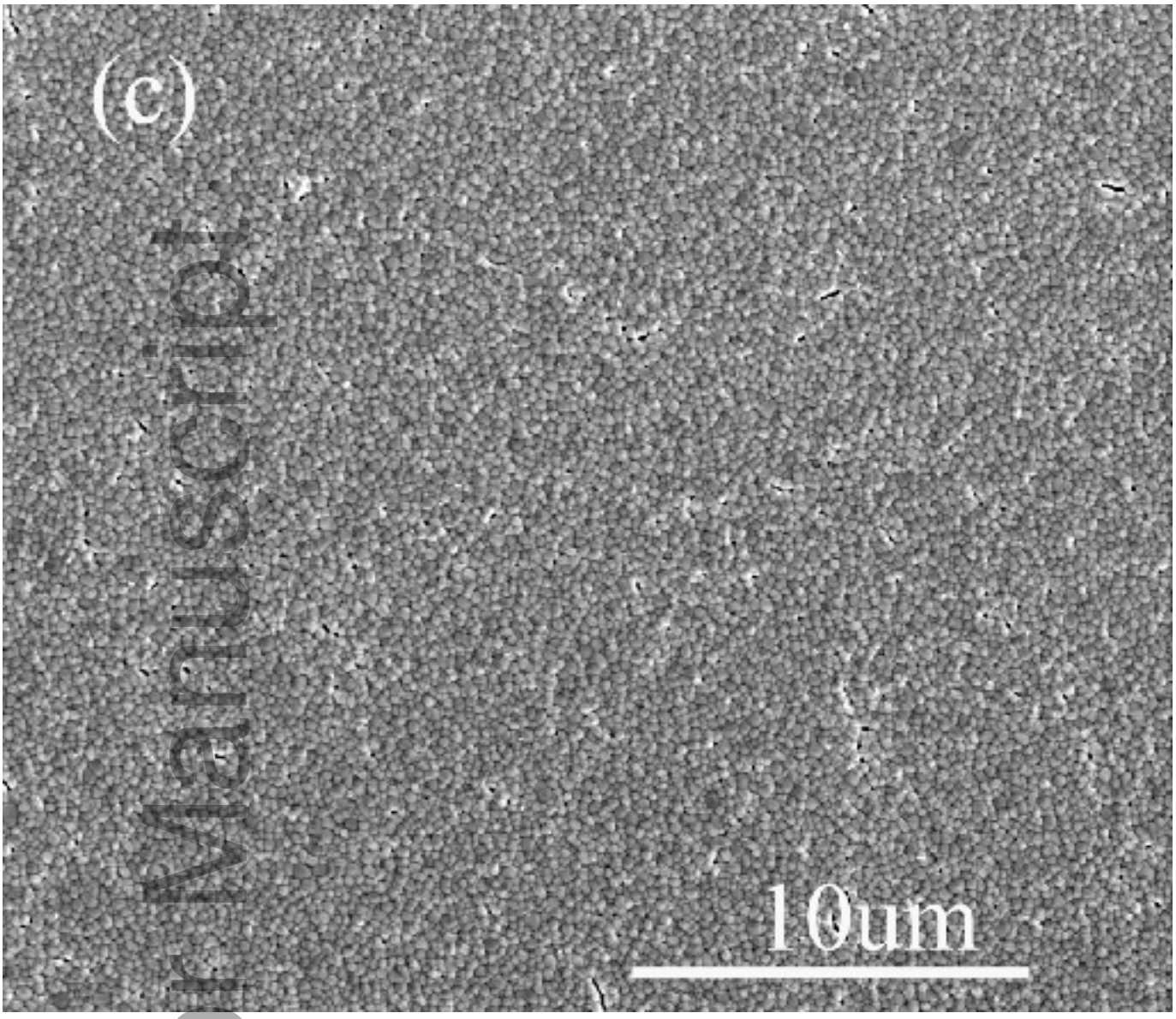

jace_16392_f4ï¼ˆcï¼‰-1.tif

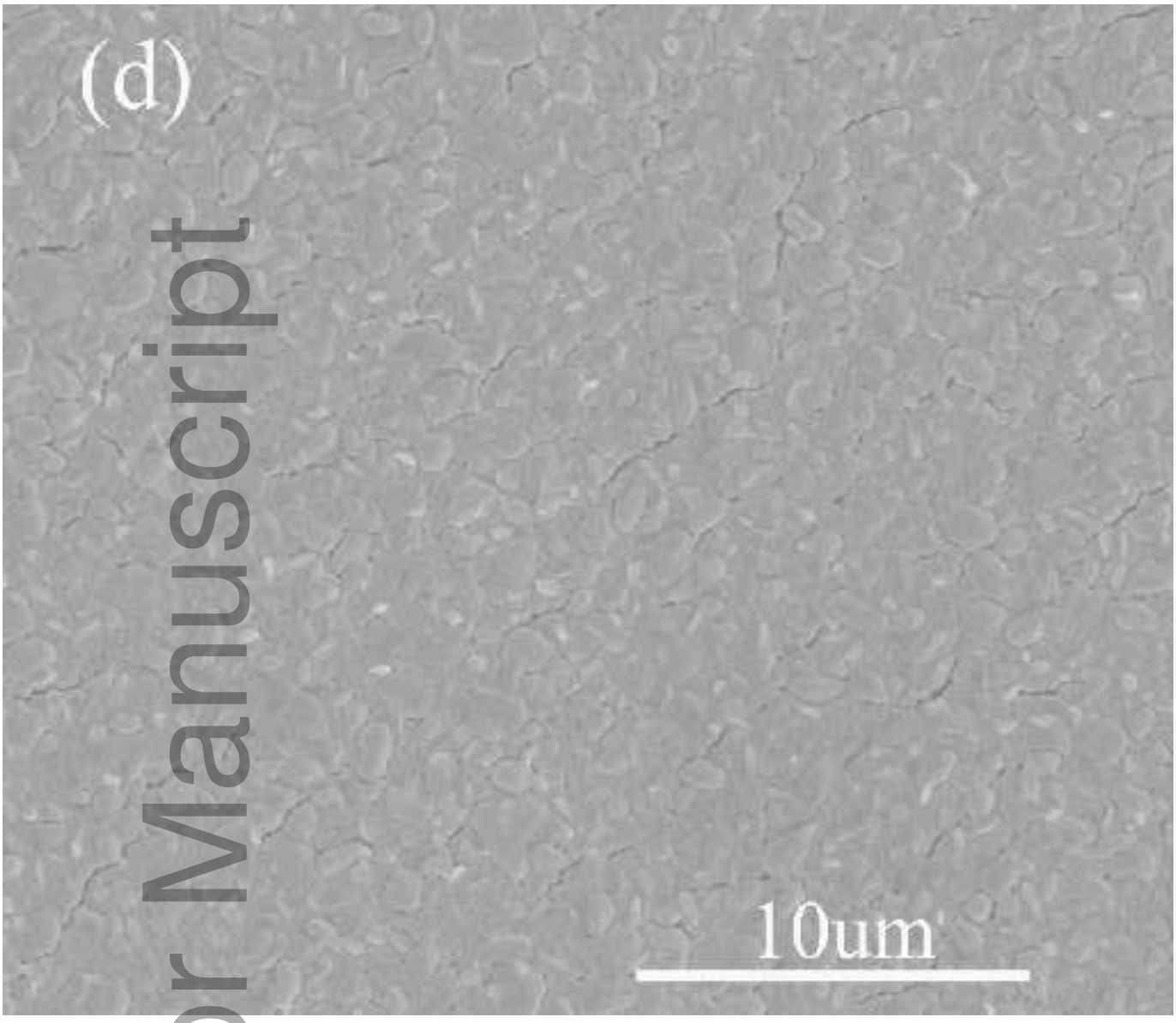

jace_16392_f4ï¼ˆdï¼‰-1.tif

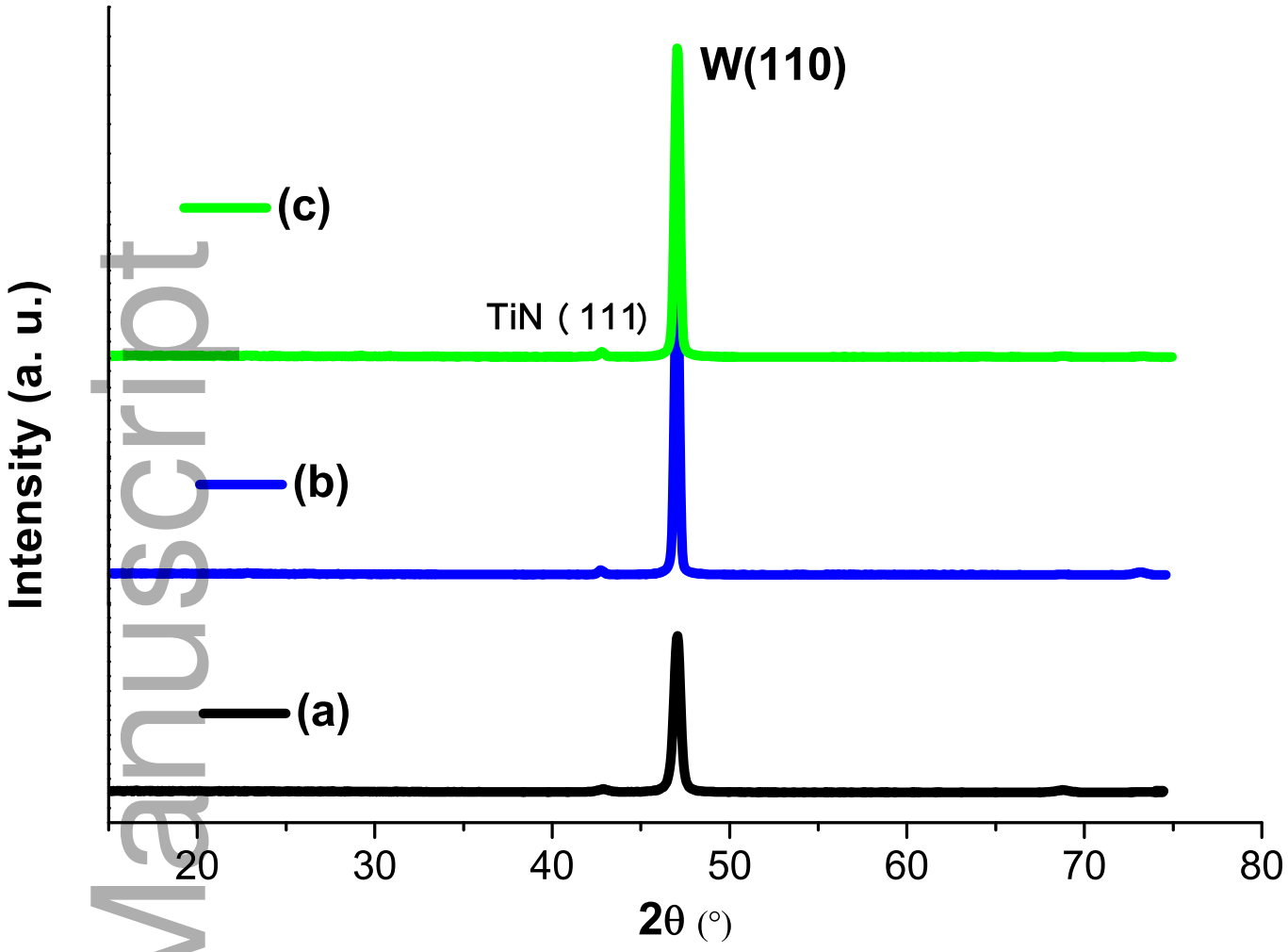

jace_16392_f5.eps

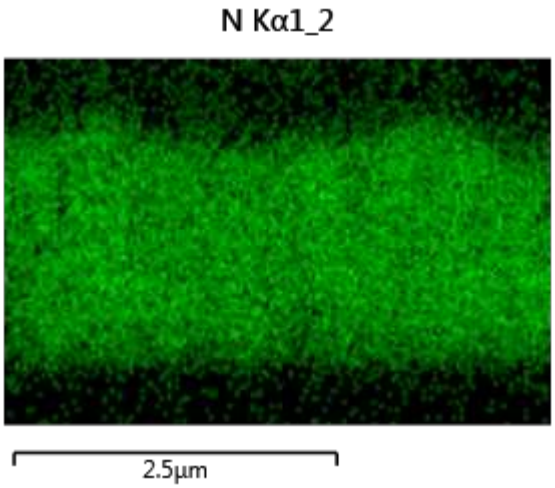

jace_16392_f6-n.tif

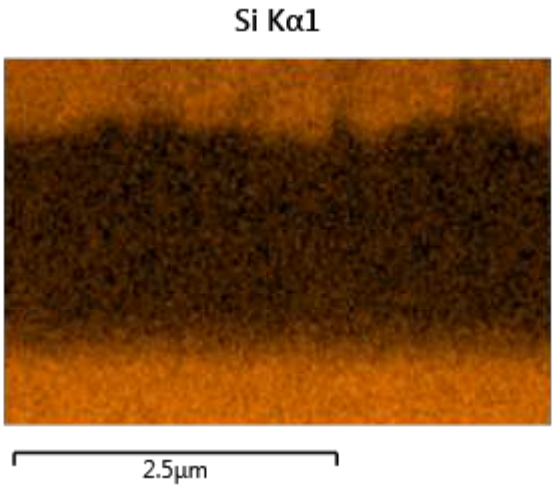

jace_16392_f6-si.tif

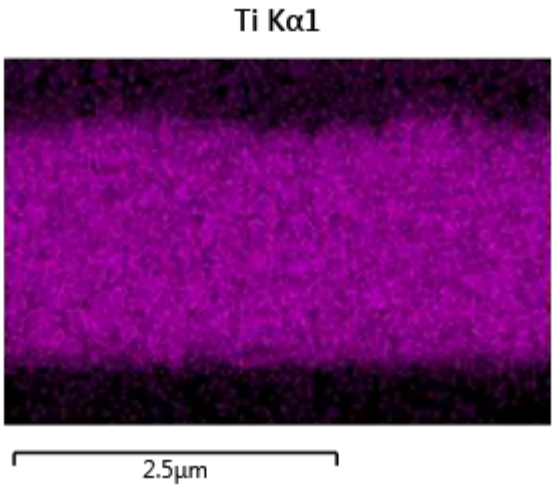

jace_16392_f6-ti.tif

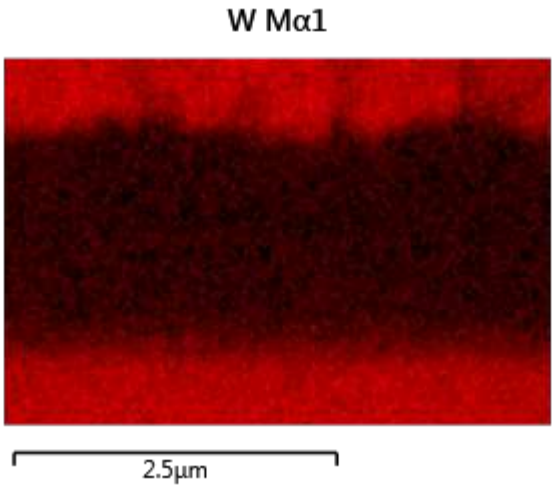

jace_16392_f6-w.tif

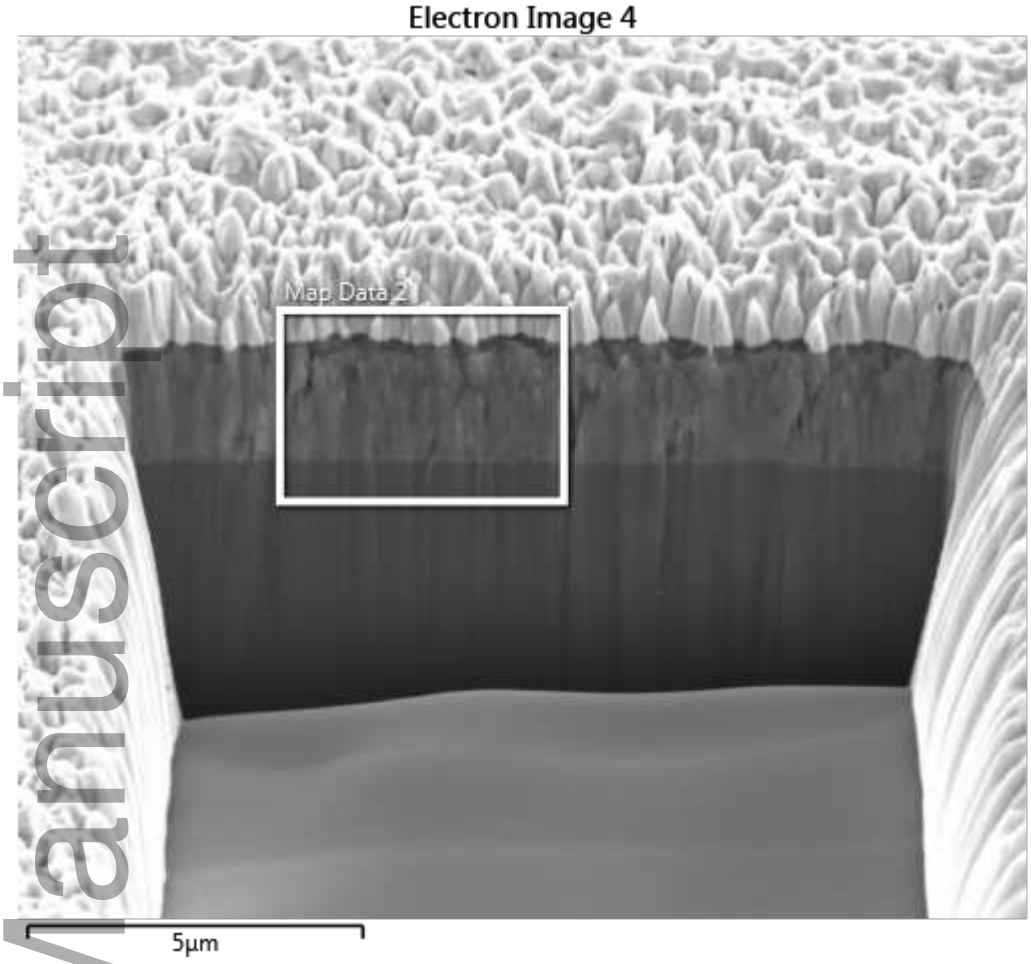

jace_16392_f6.tif

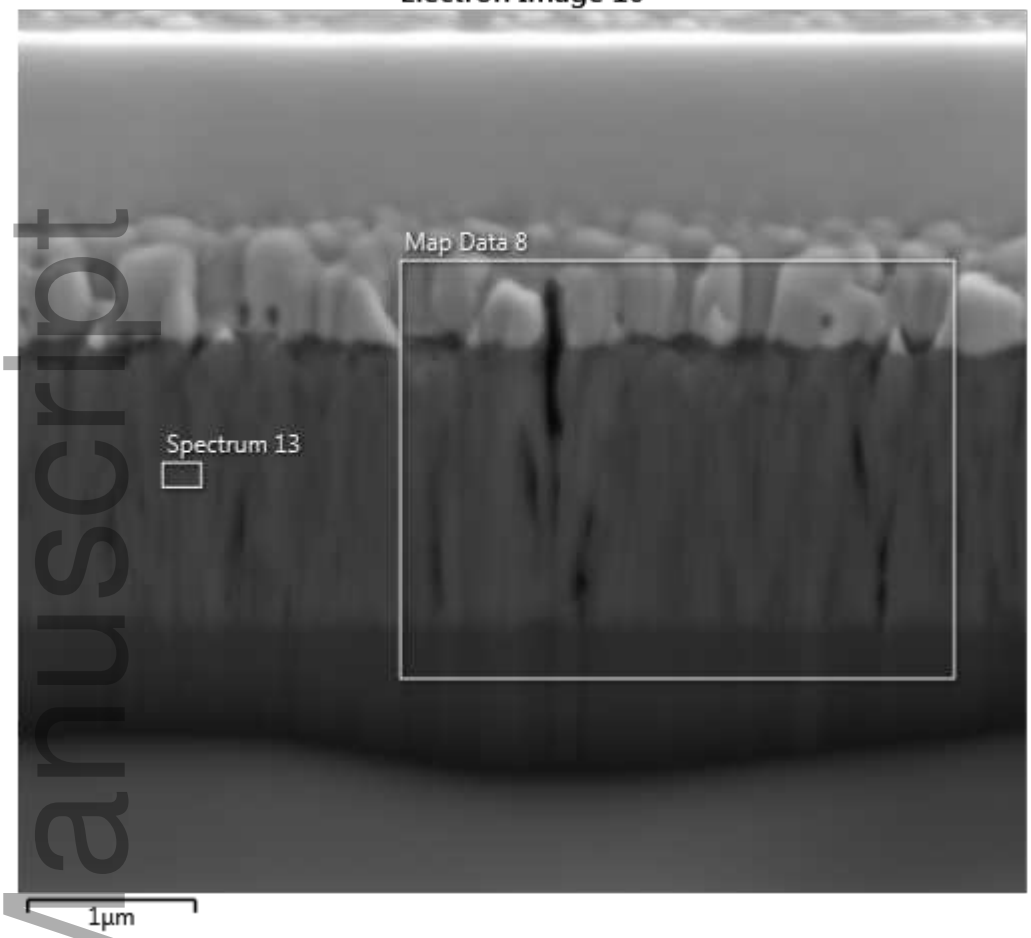

jace_16392_f7.tif

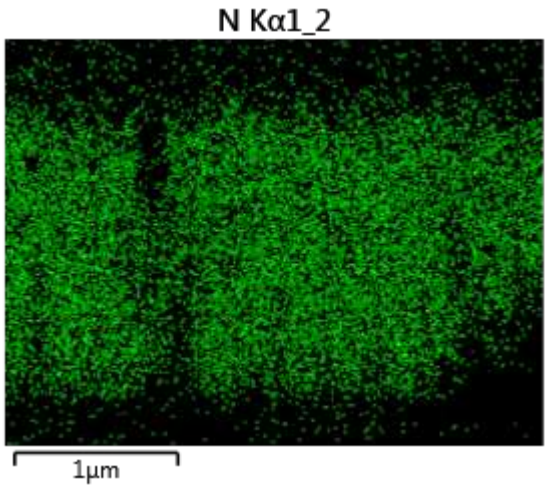

jace_16392_f7_n.tif

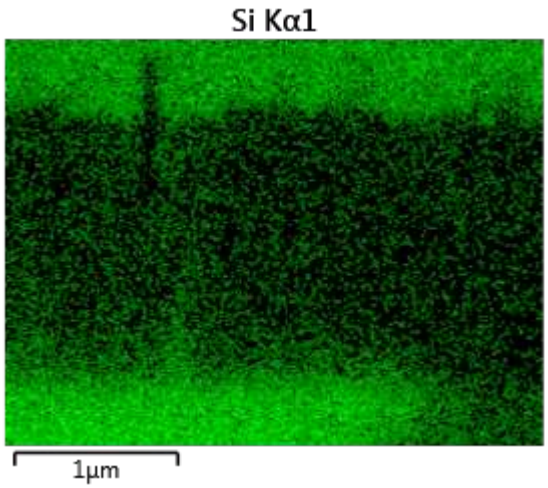

jace_16392_f7_si.tif

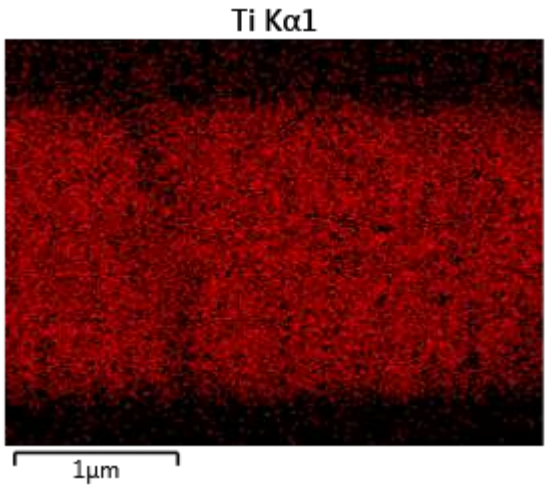

jace_16392_f7_ti.tif

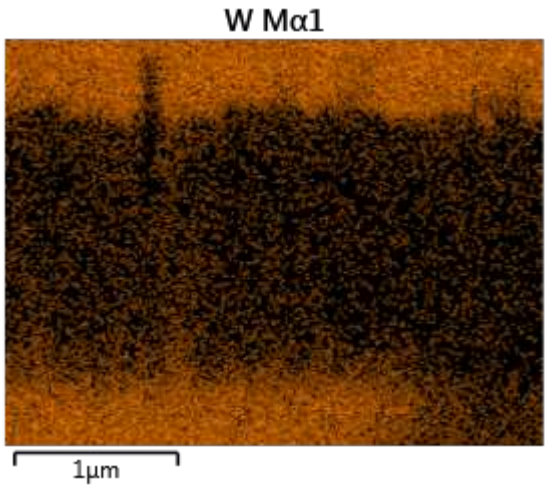

jace_16392_f7_w.tif